

Fast-GANFIT: Generative Adversarial Network for High Fidelity 3D Face Reconstruction

Baris Gecer, Stylianos Ploumpis, Irene Kotsia, and Stefanos Zafeiriou,

Abstract—A lot of work has been done towards reconstructing the 3D facial structure from single images by capitalizing on the power of Deep Convolutional Neural Networks (DCNNs). In the recent works, the texture features either correspond to components of a linear texture space or are learned by auto-encoders directly from in-the-wild images. In all cases, the quality of the facial texture reconstruction is still not capable of modeling facial texture with high-frequency details. In this paper, we take a radically different approach and harness the power of Generative Adversarial Networks (GANs) and DCNNs in order to reconstruct the facial texture and shape from single images. That is, we utilize GANs to train a very powerful facial texture prior from a large-scale 3D texture dataset. Then, we revisit the original 3D Morphable Models (3DMMs) fitting making use of non-linear optimization to find the optimal latent parameters that best reconstruct the test image but under a new perspective. In order to be robust towards initialisation and expedite the fitting process, we propose a novel self-supervised regression based approach. We demonstrate excellent results in photorealistic and identity preserving 3D face reconstructions and achieve for the first time, to the best of our knowledge, facial texture reconstruction with high-frequency details.

arXiv:2105.07474v1 [cs.CV] 16 May 2021

1 INTRODUCTION

ESTIMATION of the 3D facial surface and other intrinsic components of the face from single images (*e.g.*, albedo) is a very important problem at the intersection of computer vision and machine learning with countless applications (*e.g.*, face recognition, face editing, virtual reality). It is now twenty years from the seminal work of Blanz and Vetter [4] which showed that it is possible to reconstruct shape and albedo by solving a non-linear optimization problem that is constrained by linear statistical models of facial texture and shape. This statistical model of texture and shape is called a 3D Morphable Model (3DMM). Arguably the most popular publicly available 3DMM is the Basel model built from 200 people [26]. Recently, large scale statistical models of face and head shape have been made publicly available [7], [10], [32], [37], [48], and some studies even proposed to learn 3DMMs from in-the-wild images and videos [18], [49], [55], [57].

For many years 3DMMs and its variants were the methods of choice for 3D face reconstruction [14], [27], [41], [62]. Furthermore, with appropriate statistical texture models on image features such as Scale Invariant Feature Transform (SIFT) and Histogram Of Gradients (HOG), 3DMM-based methodologies can still achieve state-of-the-art performance in 3D shape estimation on images captured under unconstrained conditions [6]. Nevertheless, those methods [6] can reconstruct only the shape and not the facial texture. Another line of research in [42], [61] decouples texture and shape reconstruction. A standard linear 3DMM fitting strategy [53] is used for face reconstruction followed by a number of steps for texture completion and refinement. In these papers [42], [61], the texture looks excellent when rendered under professional renderers (*e.g.*, Arnold), nevertheless when the texture is overlaid on the images the quality significantly drops¹.

In the past two years, a lot of work has been conducted on how to harness Deep Convolutional Neural Networks (DCNNs) for 3D shape and texture reconstruction. The first such methods either trained regression DCNNs from image to the parameters of

a 3DMM [43], [54] or used a 3DMM to synthesize images [22], [38] and formulate an image-to-image translation problem using DCNNs to estimate the depth² [45]. The more recent unsupervised DCNN-based methods are trained to regress 3DMM parameters from identity features by making use of differentiable image formation architectures [9] and differentiable renderers [20], [39], [50], [52].

The most recent methods such as [15], [51], [56] use both the 3DMM model, as well as additional network structures (called correctives) in order to extend the shape and texture representation. Even though the paper [51] shows that the reconstructed facial texture has indeed more details than a texture estimated from a 3DMM [52], [54], it is still unable to capture high-frequency details in texture and subsequently many identity characteristics (please see the Fig. 6). Furthermore, because the method permits the reconstructions to be outside the 3DMM space, it is susceptible to outliers (*e.g.*, glasses) which are baked in shape and texture. Although neural rendering networks (*i.e.* trained by VAE [33]) generates outstanding quality textures, each network is capable of storing up to few individuals whom should be placed in a controlled environment to collect ~ 20 millions of images.

In this paper³, we still propose to build upon the success of DCNNs but take a radically different approach for 3D shape and texture reconstruction from a single in-the-wild image. That is, instead of formulating regression methodologies or auto-encoder structures that make use of self-supervision [20], [51], [56], we revisit the optimization-based 3DMM fitting approach by the supervision of deep identity features and by training a Generative Adversarial Network (GAN) on a large-scale 3D texture dataset as our statistical parametric representation of the facial texture. Furthermore, we propose a novel self-supervised approach that learns a regression network which can be used for initialisation. We show that by using this approach we can considerably expedite

2. The depth was afterwards refined by fitting a 3DMM and then changing the normals by using image features.

3. Project page: <https://github.com/barisgecer/ganfit>

Manuscript received April 19, 2005; revised August 26, 2015.

1. Please see Fig. 12 for a comparison with [42], [61].

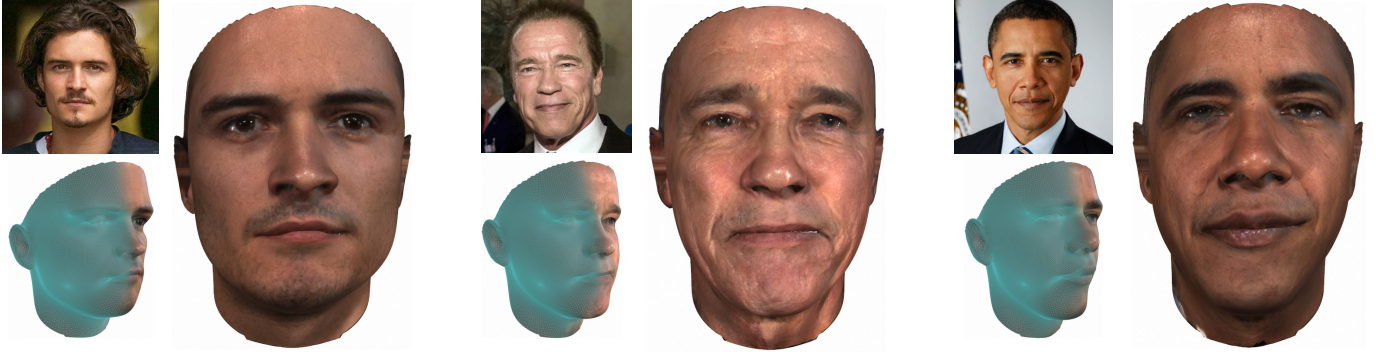


Fig. 1: The proposed deep fitting approach can reconstruct high quality texture and geometry from a single image with precise identity recovery. The reconstructions in the figure and the rest of the paper are represented by a vector of size 700 floating points and rendered without any special effects. We would like to highlight that the depicted texture is reconstructed by our model and none of the features taken directly from the image.

fitting of the model.

In particular, the novelties that this paper brings are:

- We show for the first time, to the best of our knowledge, that a large-scale high-resolution statistical reconstruction of the complete facial surface on an unwrapped UV space can be successfully used for reconstruction of arbitrary facial textures even captured in unconstrained recording conditions⁴.
- We formulate a novel 3DMM fitting strategy which is based on GANs and a differentiable renderer.
- We devise a novel cost function which combines various content losses on deep identity features from a face recognition network.
- We demonstrate excellent facial shape and texture reconstructions in arbitrary recording conditions that are shown to be both photorealistic and identity preserving in qualitative and quantitative experiments.

A preliminary version of the paper has appeared in [19]. In particular, one drawback of our earlier approach [19] is its sensitivity to the initialization of the generated texture which may or may not lead to the global minima and sometimes result in sub-optimal reconstructions. In this paper we propose a new self-supervised regression framework that can be used for initialisation. In particular, in order to initialize *GANFit* optimization parameters closer to global/good minima, we propose to train an regressor network. This is achieved by designing a self-supervised learning pipeline where, given an input image, the encoder network regresses *GANFit* latent parameters, that trained by the same image formation and loss functions as *GANFit*. The resulting network can either regress 3D reconstruction parameters directly (called *FastGANFit*) or initialize *GANFit*'s latent parameters by the regressed parameters before running *GANFit* optimization (called *GANFit++*). This combination of optimization- and regression-based 3D reconstruction leverage best of both worlds: stability of inference and high-fidelity of iterative optimization [17]. Furthermore, one can also enjoy flexibility of trade-off between

4. In the very recent works, it was shown that it is feasible to reconstruct the non-visible parts a UV space for facial texture completion [11] and that GANs can be used to generate novel high-resolution faces [47]. Nevertheless, our work is the first one that demonstrates that a GAN can be used as powerful statistical texture prior and reconstruct the complete texture of arbitrary facial images.

speed and quality depending on the application. In summary, *GANFit++* offers large improvement over the approach proposed in our preliminary work [19].

The rest of paper is organised as follows: in Sec. 2.1.1 we provide an overview of 3DMM fitting approaches in the literature. In Sec. 3, we describe *GANFit* approach as in [19] and we propose the improvements over it in Sec. 4 including *FastGANFit*. Experimental results are provided in Sec. 5. Conclusions are drawn in Sec. 6.

2 HISTORY OF 3DMM FITTING

Our methodology naturally extends and generalizes the ideas of texture and shape 3DMM using modern methods for representing texture using GANs, as well as defines loss functions using differentiable renderers and very powerful publicly available face recognition networks [12]. Before we define our cost function, we will briefly outline the history of 3DMM representation and fitting.

2.1 3DMM representation

The first step is to establish dense correspondences between the training 3D facial meshes and a chosen template with fixed topology in terms of vertices and triangulation.

2.1.1 Texture

Traditionally 3DMMs use a UV map for representing texture. UV maps help us to assign 3D texture data into 2D planes with universal per-pixel alignment for all textures. A commonly used UV map is built by cylindrical unwrapping the mean shape into a 2D flat space formulation, which we use to create an RGB image \mathbf{I}_{UV} . Each vertex in the 3D space has a texture coordinate t_{coord} in the UV image plane in which the texture information is stored. A universal function exists, where for each vertex we can sample the texture information from the UV space as $\mathbf{T} = \mathcal{P}(\mathbf{I}_{UV}, t_{coord})$.

In order to define a statistical texture representation, all the training texture UV maps are vectorized and Principal Component Analysis (PCA) is applied. Under this model any test texture \mathbf{T}^0 is approximated as a linear combination of the mean texture \mathbf{m}_t and a set of bases \mathbf{U}_t as follows:

$$\mathbf{T}(\mathbf{p}_t) \approx \mathbf{m}_t + \mathbf{U}_t \mathbf{p}_t \quad (1)$$

where \mathbf{p}_t is the texture parameters for the text sample \mathbf{T}^0 . In the early 3DMM studies, the statistical model of the texture was built with few faces captured in strictly controlled conditions and was used to reconstruct the test albedo of the face. Since, such texture models can hardly represent faces captured in uncontrolled recording conditions (in-the-wild). Recently it was proposed to use statistical models of hand-crafted features such as SIFT or HoG [6] directly from in-the-wild faces. The interested reader is referred to [5], [40] for more details on texture models used in 3DMM fitting algorithms.

The recent 3D face fitting methods [15], [51], [56] still make use of similar statistical models for the texture. Hence, they can naturally represent only the low-frequency components of the facial texture (please see Fig. 6).

2.1.2 Shape

The method of choice for building statistical models of facial or head 3D shapes is still PCA [28]. Assuming that the 3D shapes in correspondence comprise of N vertexes, *i.e.*, $\mathbf{s} = [\mathbf{x}_1^T, \dots, \mathbf{x}_N^T]^T = [x_1, y_1, z_1, \dots, x_N, y_N, z_N]^T$. In order to represent both variations in terms of identity and expression, generally two linear models are used. The first is learned from facial scans displaying the neutral expression (*i.e.*, representing identity variations) and the second is learned from displacement vectors (*i.e.*, representing expression variations). Then a test facial shape $\mathbf{S}(\mathbf{p}_{s,e})$ can be written as

$$\mathbf{S}(\mathbf{p}_{s,e}) \approx \mathbf{m}_{s,e} + \mathbf{U}_{s,e}\mathbf{p}_{s,e} \quad (2)$$

where $\mathbf{m}_{s,e}$ is the mean shape vector, $\mathbf{U}_{s,e} \in \mathbb{R}^{3N \times n_{s,e}}$ is $\mathbf{U}_{s,e} = [\mathbf{U}_s, \mathbf{U}_e]$ where the \mathbf{U}_s are the basis that correspond to identity variations, and \mathbf{U}_e the basis that correspond to expression. Finally, $\mathbf{p}_{s,e}$ are the $n_{s,e}$ shape parameters which can be split accordingly to the identity and expression bases: $\mathbf{p}_{s,e} = [\mathbf{p}_s, \mathbf{p}_e]$. Please note that all basis matrices are scaled with their corresponding eigenvalues.

2.2 Fitting

3D face and texture reconstruction by fitting a 3DMM is performed by solving a non-linear energy based cost optimization problem that recovers a set of parameters $\mathbf{p} = [\mathbf{p}_{s,e}, \mathbf{p}_t, \mathbf{p}_c, \mathbf{p}_l]$ where \mathbf{p}_c are the parameters related to a camera model and \mathbf{p}_l are the parameters related to an illumination model. The optimization can be formulated as:

$$\min_{\mathbf{p}} \mathcal{E}(\mathbf{p}) = \|\mathbf{I}^0(\mathbf{p}) - \mathbf{W}(\mathbf{p})\|_2^2 + \text{Reg}(\{\mathbf{p}_{s,e}, \mathbf{p}_l\}) \quad (3)$$

where \mathbf{I}^0 is the test image to be fitted and \mathbf{W} is a vector produced by a physical image formation process (*i.e.*, rendering) controlled by \mathbf{p} . Finally, Reg is the statistical regularization term in order to avoid overfitting for a particular pose, illumination *etc.* This term constrains the model parameters in a plausible spectrum by pushing them closer to the parameters of the mean face, and can be formulated as follows:

$$\text{Reg}(\mathbf{p}_*) = \sum \mathbf{p}_*^2 \quad (4)$$

Various methods have been proposed for numerical optimization of the above cost functions [2], [24]. A notable recent approach is [6] which uses handcrafted features (*i.e.*, \mathbf{H}) for texture representation simplified the cost function as:

$$\min_{\mathbf{p}^r} \mathcal{E}(\mathbf{p}^r) = \|\mathbf{H}(\mathbf{I}^0(\mathbf{p}^r)) - \mathbf{H}(\mathbf{W}(\mathbf{p}^r))\|_A^2 + \text{Reg}(\mathbf{p}_{s,e}) \quad (5)$$

where $\|\mathbf{a}\|_A^2 = \mathbf{a}^T \mathbf{A} \mathbf{a}$, \mathbf{A} is the orthogonal space to the statistical model of the texture and \mathbf{p}^r is the set of reduced parameters $\mathbf{p}^r = \{\mathbf{p}_{s,e}, \mathbf{p}_c\}$. The optimization problem in Eq. 5 is solved by Gauss-Newton method. The main drawback of this method is that the facial texture is not reconstructed.

In this paper, we generalize the 3DMM fittings and introduce the following novelties:

- We use a GAN on high-resolution UV maps as our statistical representation of the facial texture. That way we can reconstruct textures with high-frequency details.
- Instead of other cost functions used in the literature such as low-level ℓ_1 or ℓ_2 loss (*e.g.*, RGB values [36], edges [41]) or hand-crafted features (*e.g.*, SIFT [6]), we propose a novel cost function that is based on feature loss from the various layers of publicly available face recognition embedding network [12]. Unlike others, deep identity features are very powerful at preserving identity characteristics of the input image.
- We replace physical image formation stage with a differentiable renderer to make use of first order derivatives (*i.e.*, gradient descent). Unlike its alternatives, gradient descent provides computationally cheaper and more reliable derivatives through such deep architectures (*i.e.*, above-mentioned texture GAN and identity DCNN).

3 APPROACH

We propose an optimization-based 3D face reconstruction approach from a single image that employs a high fidelity texture generation network as statistical prior as illustrated in Fig. 2. To this end, the reconstruction mesh is formed by 3D morphable shape model; textured by the generator network's output UV map; and projected into 2D image by a differentiable renderer. The distance between the rendered image and the input image is minimized in terms of a number of cost functions by updating the latent parameters of 3DMM and the texture network with gradient descent. We mainly formulate these functions based on rich features of face recognition network [12], [35], [44] for smoother convergence and landmark detection network [13] for alignment and rough shape estimation.

The following sections introduce firstly our novel texture model that employs a generator network trained by progressive growing GAN framework. After describing the procedure for image formation with differentiable renderer, we formulate our cost functions and the procedure for fitting our shape and texture models onto a test image.

3.1 GAN Texture Model

Although conventional PCA is powerful enough to build a decent shape and texture model, it is often unable to capture high frequency details and ends up having blurry textures due to its Gaussian nature. This becomes more apparent in texture modelling which is a key component in 3D reconstruction to preserve identity as well as photo-realism.

GANs are shown to be very effective at capturing such details. However, they suffer from preserving 3D coherency [21] of the target distribution when the training images are semi-aligned. We found that a GAN trained with UV representation of real textures with per pixel alignment avoids this problem and better captures

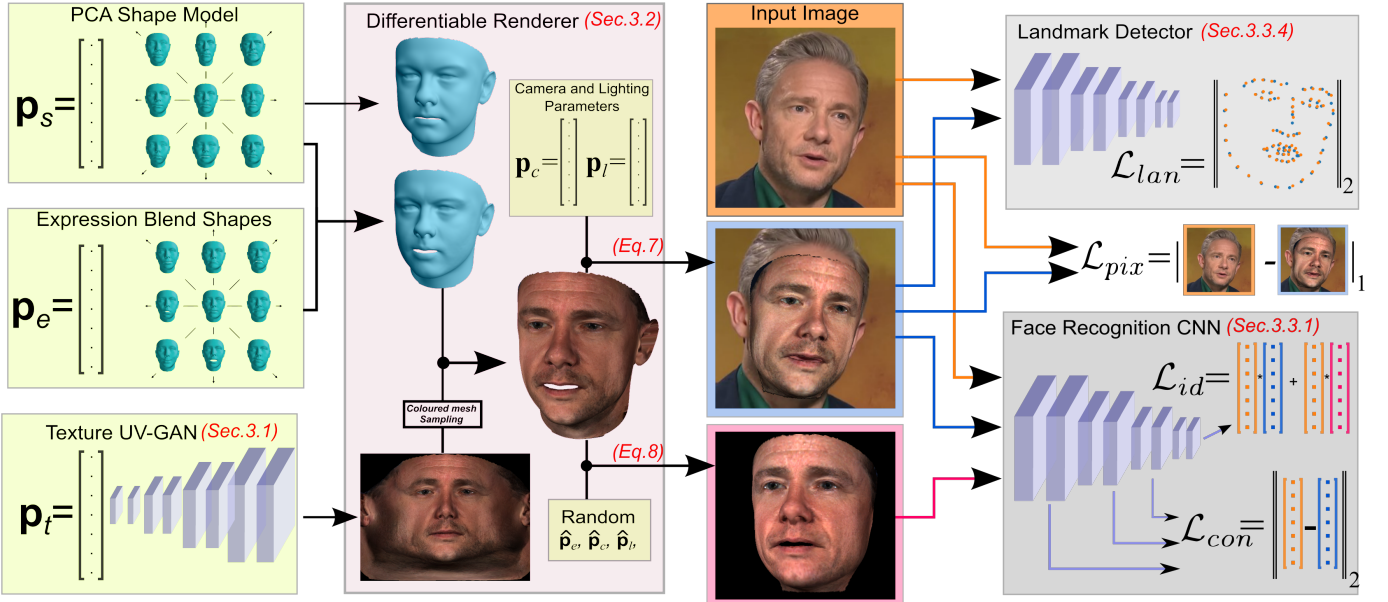


Fig. 2: Detailed overview of the proposed approach. A 3D face reconstruction is rendered by a differentiable renderer (shown in purple). Cost functions are mainly formulated by means of identity features on a pretrained face recognition network (shown in gray) and they are optimized by flowing the error all the way back to the latent parameters (p_s, p_e, p_t, c, i , shown in green) with gradient descent optimization. End-to-end differentiable architecture enables us to use computationally cheap and reliable first order derivatives for optimization thus making it possible to employ deep networks as a generator (*i.e.*, statistical model) or as a cost function.

the characteristics of the training set. These findings are discussed in Sec. 5.4.2 and Table 2.

In order to take advantage of this perfect harmony, we train a progressive growing GAN [29] to model distribution of UV representations of 10,000 high resolution textures and use the trained generator network

$$\mathcal{G}(\mathbf{p}_t) : \mathbb{R}^{512} \rightarrow \mathbb{R}^{H \times W \times C} \quad (6)$$

as texture model that replaces 3DMM texture model in Eq. 1.

While fitting with linear models, *i.e.*, 3DMM, is as simple as linear transformation, fitting with a generator network can be formulated as an optimization that minimizes per-pixel Manhattan distance between target texture in UV space \mathbf{I}_{uv} and the network output $\mathcal{G}(\mathbf{p}_t)$ with respect to the latent parameter \mathbf{p}_t , *i.e.*, $\min_{\mathbf{p}_t} |\mathcal{G}(\mathbf{p}_t) - \mathbf{I}_{uv}|$.

3.2 Differentiable Renderer

Following [20], we employ a differentiable renderer to project 3D reconstruction into a 2D image plane based on deferred shading model with given camera and illumination parameters. Since color and normal attributes at each vertex are interpolated at the corresponding pixels with barycentric coordinates, gradients can be easily backpropagated through the renderer to the latent parameters.

A 3D textured mesh at the center of Cartesian origin $[0, 0, 0]$ is projected onto 2D image plane by a pinhole camera model with the camera standing at $[x_c, y_c, z_c]$, directed towards $[x'_c, y'_c, z'_c]$, with world's up direction $[\hat{x}_c, \hat{y}_c, \hat{z}_c]$, and with the focal length f_c . The illumination is modelled by phong shading given 1) direct light source at 3D coordinates $[x_l, y_l, z_l]$ with color values $[r_l, g_l, b_l]$, and 2) color of ambient lighting $[r_a, g_a, b_a]$.

Finally, we denote the rendered image given geometry ($\mathbf{p}_{s,e}$), texture (\mathbf{p}_t), camera ($\mathbf{p}_c = [x_c, y_c, z_c, x'_c, y'_c, z'_c, \hat{x}_c, \hat{y}_c, \hat{z}_c, f_c]$) and lighting parameters ($\mathbf{p}_l = [x_l, y_l, z_l, r_l, g_l, b_l, r_a, g_a, b_a]$) by the following:

$$\mathbf{I}^R = \mathcal{R}(\mathbf{S}(\mathbf{p}_s, \mathbf{p}_e), \mathcal{P}(\mathcal{G}(\mathbf{p}_t)), \mathbf{p}_c, \mathbf{p}_l) \quad (7)$$

where we construct shape mesh by 3DMM as given in Eq. 2 and texture by GAN generator network as in Eq. 6. Since our differentiable renderer supports only color vectors, we sample from our generated UV map to get vectorized color representation as explained in Sec. 2.1.1.

Additionally, we render a secondary image with random expression, pose and illumination in order to generalize identity related parameters well with those variations. We sample expression parameters from a normal distribution as $\hat{\mathbf{p}}_e \sim \mathcal{N}(\mu = 0, \sigma = 0.5)$ and sample camera and illumination parameters from the Gaussian distribution of 300W-3D dataset as $\hat{\mathbf{p}}_c \sim \mathcal{N}(\hat{\mu}_c, \hat{\sigma}_c)$ and $\hat{\mathbf{p}}_l \sim \mathcal{N}(\hat{\mu}_l, \hat{\sigma}_l)$. This rendered image of the same identity as \mathbf{I}^R (*i.e.*, with same \mathbf{p}_s and \mathbf{p}_t parameters) is expressed by the following:

$$\hat{\mathbf{I}}^R = \mathcal{R}(\mathbf{S}(\mathbf{p}_s, \hat{\mathbf{p}}_e), \mathcal{P}(\mathcal{G}(\mathbf{p}_t)), \hat{\mathbf{p}}_c, \hat{\mathbf{p}}_l) \quad (8)$$

3.3 Cost Functions

Given an input image \mathbf{I}^0 , we optimize all of the aforementioned parameters simultaneously with gradient descent updates. In each iteration, we simply calculate the forthcoming cost terms for the current state of the 3D reconstruction, and take the derivative of the weighted error with respect to the parameters using backpropagation.

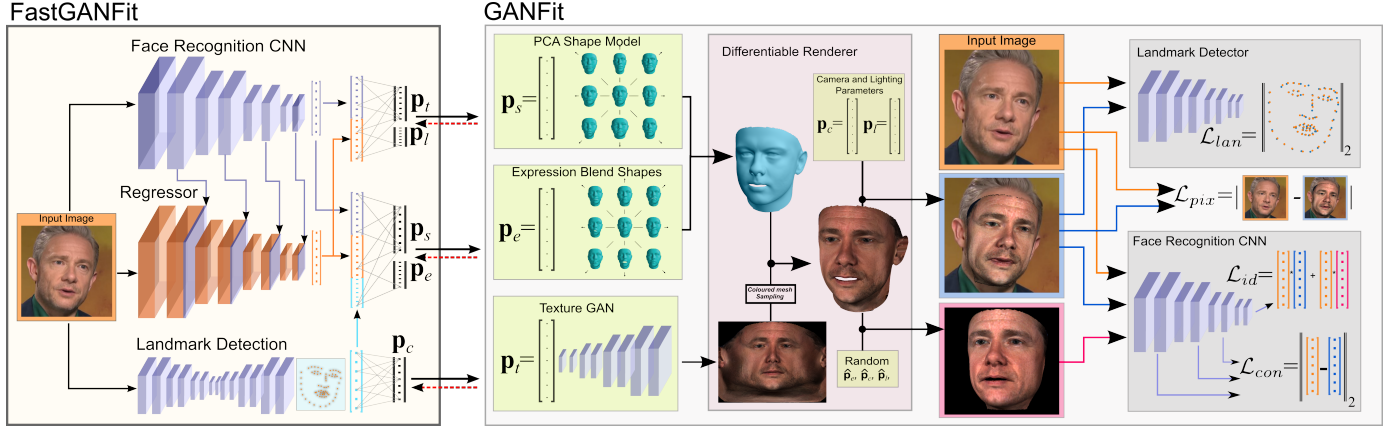


Fig. 3: Overview of the approach with regression network. The network is end-to-end connected with the differentiable renderer and the loss functions of *GANFit*. It benefits from the activations of all layers of a pretrained face recognition network and detection of a hourglass landmark detector. The network is trained similar to *GANFit* optimization: 1) alignment 2) full objective. The only difference is that now the regression network is being optimized instead of the trainable latent parameters of *GANFit*.

3.3.1 Identity Loss

With the availability of large scale datasets, CNNs have shown incredible performance on many face recognition benchmarks. Their strong identity features are robust to many variations including pose, expression, illumination, age *etc.* These features are shown to be quite effective at many other tasks including novel identity synthesizing [16], face normalization [9] and 3D face reconstruction [20]. In our approach, we take advantage of an off-the-shelf state-of-the-art face recognition network [12]⁵ in order to capture identity related features of an input face image and optimize the latent parameters accordingly. More specifically, given a pretrained face recognition network $\mathcal{F}^n(\mathbf{I}) : \mathbb{R}^{H \times W \times C} \rightarrow \mathbb{R}^{512}$ consisting of n convolutional filters, we calculate the cosine distance between the identity features (*i.e.*, embeddings) of the real target image and our rendered images as following:

$$\mathcal{L}_{id} = 1 - \frac{\mathcal{F}^n(\mathbf{I}^0) \cdot \mathcal{F}^n(\mathbf{I}^R)}{\|\mathcal{F}^n(\mathbf{I}^0)\|_2 \|\mathcal{F}^n(\mathbf{I}^R)\|_2} \quad (9)$$

We formulate an additional identity loss on the rendered image $\hat{\mathbf{I}}^R$ that is rendered with random pose, expression and lighting. This loss ensures that our reconstruction resembles the target identity under different conditions. We formulate it by replacing \mathbf{I}^R by $\hat{\mathbf{I}}^R$ in Eq. 9 and it is denoted as $\hat{\mathcal{L}}_{id}$.

3.3.2 Content Loss

Face recognition networks are trained to remove all kinds of attributes (*e.g.*, expression, illumination, age, pose) other than abstract identity information throughout the convolutional layers. Despite their strength, the activations in the very last layer discard some of the mid-level features that are useful for 3D reconstruction, *e.g.*, variations that depend on age. Therefore we found it effective to accompany identity loss by leveraging intermediate representations in the face recognition network that are still robust to pixel-level deformations and not too abstract to miss some details. To this end, normalized euclidean distance of intermediate

5. We empirically deduced that other face recognition networks work almost equally well and this choice is orthogonal to the proposed approach.

activations, namely content loss, is minimized between input and rendered image with the following loss term:

$$\mathcal{L}_{con} = \sum_j^n \frac{\|\mathcal{F}^j(\mathbf{I}^0) - \mathcal{F}^j(\mathbf{I}^R)\|_2}{H_{\mathcal{F}^j} \times W_{\mathcal{F}^j} \times C_{\mathcal{F}^j}} \quad (10)$$

3.3.3 Pixel Loss

While identity and content loss terms optimize albedo of the visible texture, lighting conditions are optimized based on pixel value difference directly. While this cost function is relatively primitive, it is sufficient to optimize lighting parameters such as ambient colors, direction, distance and color of a light source. We found that optimizing illumination parameters jointly with others helped to improve albedo of the recovered texture. Furthermore, pixel loss support identity and content loss with fine-grained texture as it supports highest available resolution while images needs to be downsampled to 112×112 before identity and content loss. The pixel loss is defined by pixel level ℓ_1 loss function as:

$$\mathcal{L}_{pix} = \|\mathbf{I}^0 - \mathbf{I}^R\|_1 \quad (11)$$

3.3.4 Landmark Loss

The face recognition network \mathcal{F} is pre-trained by the images that are aligned by similarity transformation to a fixed landmark template. To be compatible with the network, we align the input and rendered images under the same settings. However, this process disregards the aspect ratio and scale of the reconstruction. Therefore, we employ a deep face alignment network [13] $\mathcal{M}(\mathbf{I}) : \mathbb{R}^{H \times W \times C} \rightarrow \mathbb{R}^{68 \times 2}$ to detect landmark locations of the input image and align the rendered geometry onto it by updating the shape, expression and camera parameters. That is, camera parameters are optimized to align with the pose of image \mathbf{I} and geometry parameters are optimized for the rough shape estimation. As a natural consequence, this alignment drastically improves the effectiveness of the pixel and content loss, which are sensitive to misalignment between the two images.

The alignment error is achieved by point-to-point euclidean distances between detected landmark locations of the input image and 2D projection of the 3D reconstruction landmark locations that is available as meta-data of the shape model. Since landmark

locations of the reconstruction heavily depend on camera parameters, this loss is great a source of information the alignment of the reconstruction onto input image and is formulated as following:

$$\mathcal{L}_{lan} = \|\mathcal{M}(\mathbf{I}^0) - \mathcal{M}(\mathbf{I}^R)\|_2 \quad (12)$$

3.4 Model Fitting

We first roughly align our reconstruction to the input image by optimizing shape, expression and camera parameters by: $\min_{\mathbf{p}^r} \mathcal{E}(\mathbf{p}^r) = \lambda_{lan} \mathcal{L}_{lan} + \lambda_{reg} \text{Reg}(\{\mathbf{p}_{s,e}\})$. We then simultaneously optimize all of our parameters with gradient descent and backpropagation so as to minimize weighted combination of above loss terms in the following:

$$\begin{aligned} \min_{\mathbf{p}} \mathcal{E}(\mathbf{p}) = & \lambda_{id} \mathcal{L}_{id} + \hat{\lambda}_{id} \hat{\mathcal{L}}_{id} + \lambda_{con} \mathcal{L}_{con} + \lambda_{pix} \mathcal{L}_{pix} \\ & + \lambda_{lan} \mathcal{L}_{lan} + \lambda_{reg} \text{Reg}(\{\mathbf{p}_{s,e}, \mathbf{p}_l\}) \end{aligned} \quad (13)$$

where we weight each of our loss terms with λ parameters. In order to prevent our shape and expression models and lighting parameters from exaggeration to arbitrarily bias our loss terms, we regularize those parameters by $\text{Reg}(\{\mathbf{p}_{s,e}, \mathbf{p}_l\})$.

3.5 Fitting with Multiple Images (i.e. Video):

Although the proposed approach can fit a 3D reconstruction from a single image, one can take advantage of more images effectively when available, *e.g.*, from a video recording. This often helps to improve reconstruction quality under challenging conditions, *e.g.*, outdoor, low resolution. While state-of-the-art methods follow naive approaches by averaging either the reconstruction [54] or features-to-be-regressed [20] before making a reconstruction, we utilize the power of iterative optimization by averaging identity reconstruction parameters ($\mathbf{p}_s, \mathbf{p}_t$) after every iteration. For an image set $\mathbf{I} = \{\mathbf{I}^0, \mathbf{I}^1, \dots, \mathbf{I}^i, \dots, \mathbf{I}^{n_i}\}$, we reformulate our parameters as $\mathbf{p} = [\mathbf{p}_s, \mathbf{p}_e^i, \mathbf{p}_t, \mathbf{p}_c^i, \mathbf{p}_l^i]$ in which we average shape and texture parameters by the following ⁶:

$$\mathbf{p}_s = \sum_i^n \mathbf{p}_s^i, \mathbf{p}_t = \sum_i^n \mathbf{p}_t^i \quad (14)$$

4 REGRESSING PARAMETERS BY ENCODER

One weakness of the proposed *GANFit* approach is its sensitivity to the initialization of the generated texture as shown in Fig. 4. Due to the non-linear generator network and first order derivatives, optimization is not guaranteed to find the global minima and sometimes result in sub-optimal reconstructions. In order to initialize *GANFit* optimization parameters closer to global/good minima, we propose to train an encoder network to by the same image formation and loss functions that regress latent parameters (*i.e.*, p_s, p_t, p_e, p_c, p_l) from the input image.

In order to train this network N , we modify *GANFit* optimization by simply replacing trainable latent parameters \mathbf{p} by the activations of the encoder network ($\mathbf{p}^N = N(\mathbf{I}^0)$) as shown in Fig. 3. The architecture of the regression network particularly benefit from different levels of identity features (*i.e.*, content features) of a pretrained face recognition network [12] by passing and concatenating same-resolution activations in the regressor

6. Each frame in the supplementary video has been processed individually in order to show stability of the convergence of our approach. However, fitting with multiple images has shown to be useful in the experiments on MICC dataset in Sec. 5.3.1.

network. Moreover, we flatten and concatenate normalized landmark locations by a pretrained landmark detection network [13] before the final fully connected layers. This design leverage the information of the state of the art facial features and, unlike its alternatives [20], it allows the regressor network to benefit all levels of features (*i.e.*, [20] restrict the features from face recognition network to its final layer which is fully abstract and ignore state-relevant features, *e.g.*, age, facial hair). We call this regression network *FastGANFit* in the rest of the paper.

The activations of *FastGANFit* ($\mathbf{p}^N = N(\mathbf{I}^0)$) is connected with *GANFit*'s image formation and loss functions in an end-to-end manner. The network is then pre-trained for camera, shape and expression parameters by optimizing only $\min_{\mathbf{p}^N} \mathcal{E}(\mathbf{p}^N) = \lambda_{lan} \mathcal{L}_{lan} + \lambda_{reg} \text{Reg}(\{\mathbf{p}_{s,e}\})$. After having a good alignment of the reconstructions of a given training data, we train the regressor network again with our full objective function as follows:

$$\begin{aligned} \min_{\mathbf{p}^N} \mathcal{E}(\mathbf{p}^N) = & \lambda_{id} \mathcal{L}_{id} + \hat{\lambda}_{id} \hat{\mathcal{L}}_{id} + \lambda_{con} \mathcal{L}_{con} + \lambda_{pix} \mathcal{L}_{pix} \\ & + \lambda_{lan} \mathcal{L}_{lan} + \lambda_{reg} \text{Reg}(\{\mathbf{p}_{s,e}, \mathbf{p}_l\}) \end{aligned} \quad (15)$$

The resulting network can either regress 3D reconstruction parameters directly (called *FastGANFit*) or initialize *GANFit*'s latent parameters \mathbf{p} by the regressed parameters $N(\mathbf{I}^0)$ before running *GANFit* optimization as explained in Section 3. We call this initialization trick *GANFit++*. This combination of optimization- and regression-based 3D reconstruction leverage best of both worlds: stability of inference and high-fidelity of iterative optimization. Furthermore, one can also enjoy flexibility of trade-off between speed and quality depending on the application.

5 EXPERIMENTS

This section demonstrates the excellent performance of the proposed approach for 3D face reconstruction and shape recovery. We verify this by qualitative results in Figures 1, 5, qualitative comparisons with the state-of-the-art in Sec. 5.2 and quantitative experiment in Sec. 5.3. In our experiments, we evaluate the proposed approach under three different settings: 1) *GANFit*, *i.e.* Fitting with random initialization, 2) *Fast-GANFit*, *i.e.* Regressing the parameters by the regressor network, 3) *GANFit++*, *i.e.* Fitting after initializing with *FastGANFit*.

5.1 Implementation Details

For all of our experiments, a given face image is aligned to our fixed template using 68 landmark locations detected by an hourglass 2D landmark detection [13]. For the identity features, we employ ArcFace [12] network's pretrained models. For the generator network \mathcal{G} , we train a progressive growing GAN [29] with around 10,000 UV maps from [7] at the resolution of 512×512 . We use the Large Scale Face Model [7] for 3DMM shape model with $n_s = 158$ and the expression model learned from 4DFAB database [8] with $n_e = 29$. During fitting process, we optimize parameters using Adam Solver [30] with 0.01 learning rate. And we set our balancing factors as follows: $\lambda_{id} : 2.0, \hat{\lambda}_{id} : 2.0, \lambda_{con} : 50.0, \lambda_{pix} : 1.0, \lambda_{lan} : 0.001, \lambda_{reg} : \{0.05, 0.01\}$.

The regression network, as illustrated in Fig. 3, contains a backbone that is based on ResNet-50 [23] and ArcFace [12] which is also ResNet-50 based. Therefore the network consists of more than 50 millions model parameters. We initialize all parameters randomly, with 'xavier initializer' to be specific, except the last

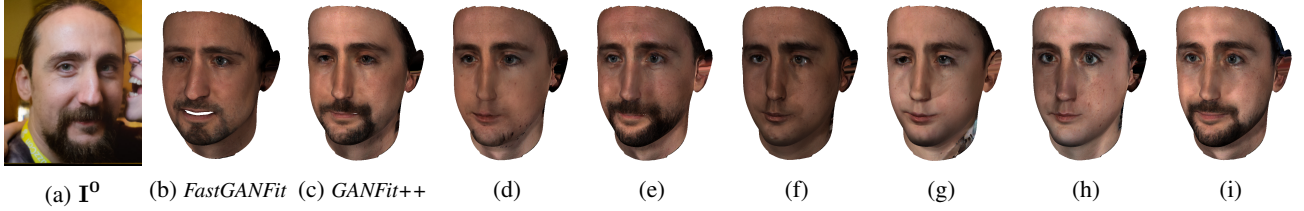


Fig. 4: An example of the proposed improvements to stabilize GANFit reconstruction. (a) The input image. (b) Estimated reconstruction by *FastGANFit*. (c) Fitting after initialization by *FastGANFit* (referred as *GANFit++*). (d-i) randomly resulting reconstructions given random initial textures (referred as *GANFit*).

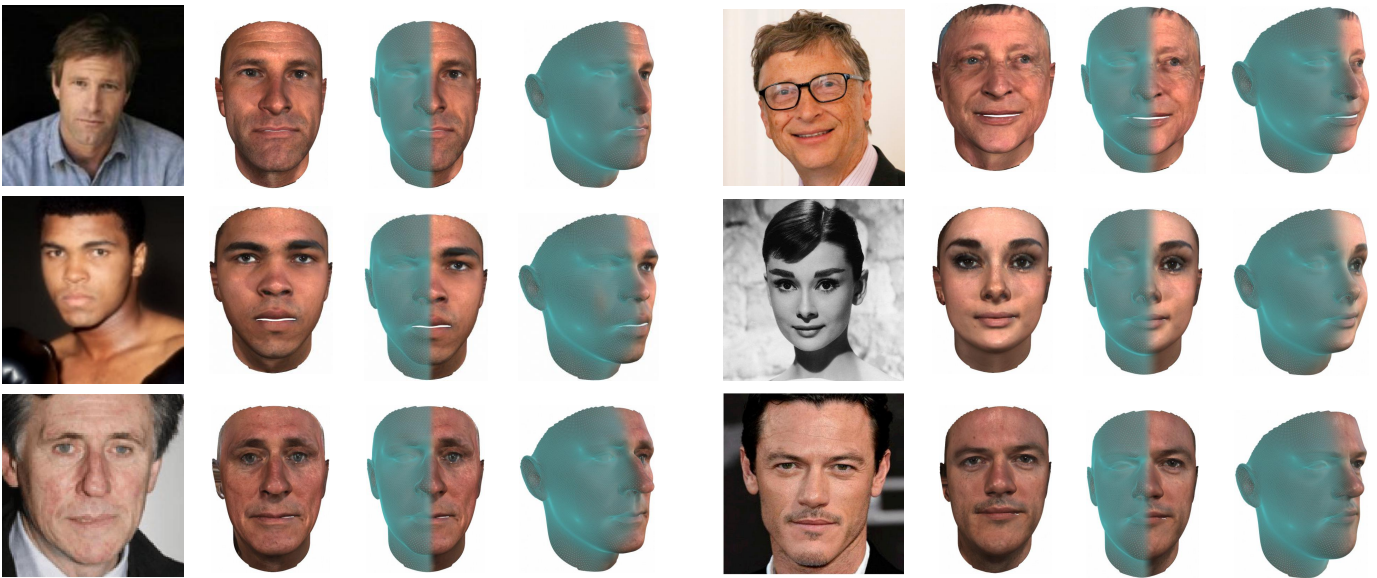


Fig. 5: Example fits of our approach for the images from various datasets. Please note that our fitting approach is robust to occlusion (e.g., glasses), low resolution and black-white in the photos and generalizes well with ethnicity, gender and age. The reconstructed textures are very well at capturing high frequency details of the identities; likewise, the reconstructed geometries from 3DMM are surprisingly good at identity preservation thanks to the identity features used, e.g., crooked nose at bottom-left, dull eyes at bottom-right and chin dimple at top-left

layers that output camera and illumination parameters. Those ones are initialized by zero initializers, and their outputs are corrected by an offset to be able to render a normal face more or less aligned with our generic alignment template and with regular lighting.

The Fitting of *GANFit* converges in around 30 seconds on an Nvidia GTX 1080 TI GPU for a single image while *FastGANFit* inference time is under a second. Since *GANFit++* is initialized closer to the minima by *FastGANFit*, it converges after 5-10 seconds.

5.2 Qualitative Results

5.2.1 Comparison on MOFA test set

Fig. 6 compares our results with the most recent face reconstruction studies [20], [51], [52], [54], [56] on a subset of MoFA test-set. The first four rows after input images show a comparison of our shape and texture reconstructions to [20], [51], [54] and the last three rows show our reconstructed geometries without texture compared to [51], [56]. All in all, our method outshines all others with its high fidelity photorealistic texture reconstructions. Both of our texture and shape reconstructions manifest strong identity characteristics of the corresponding input images from the thickness and shape of the eyebrows to wrinkles around the mouth and forehead.

Rows 2 and 5 show results of our method with and without expression fitting (i.e., \mathbf{p}_e) visualized. It is visible that our method even captured that eyelids are closed in the geometry (i.e., first column) and that the expression is well disentangled from shape compared to MoFA [52].

5.2.2 Comparison on high-quality texture generation

In order to support our claim to generate high-quality textures, in Fig. 12 we provide comparative results with [42] which renders 3D reconstruction using commercial renderer tweaks. Our method provides excellent textures even without any improvements by renderers (which is orthogonal our method). This is more visible when the reconstruction is overlaid on the input images as in Fig. 8.

5.2.3 Results under challenging conditions

Fig. 14 illustrates results of *GANFit* under more challenging conditions such as strong illuminations, self-occlusions and facial hair. Please note that our method successfully reconstruct these challenging face images in 3D thanks to strong face recognition features. Particularly, Fig. 14(d) shows that the direction and the intensity of the illumination in the scene are successfully estimated by our lighting model which consists of one RGB point light source and RGB ambient lighting. This result indicates that our

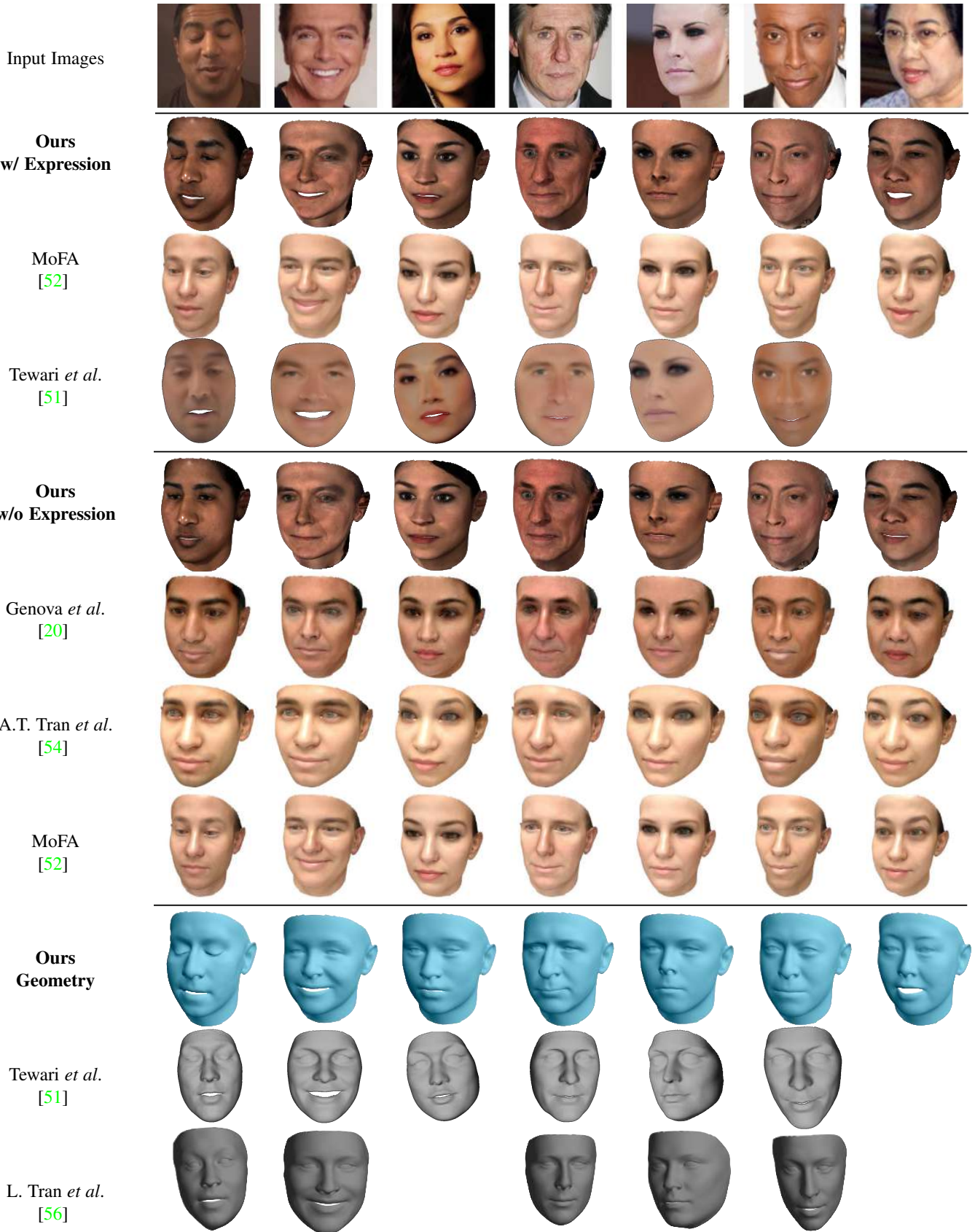


Fig. 6: Comparison of our qualitative results with other state-of-the-art methods in MoFA-Test dataset. Rows 2-4 show comparison of textured geometry with original expression, rows 5-8 show comparison of textured geometry with neutral expression and rows 9-11 compare only shapes.

	Method	Shape Estimation (mm) ↓				Identity Sim. ↑				
		Cooperative		Indoor		Outdoor		Coop. Mean	In. Mean	Out. Mean
VAE	VAEFit	1.01	± 0.24	0.93	± 0.18	1.02	± 0.26	0.90	0.88	0.82
	Fast-VAEFit	1.37	± 0.30	1.17	± 0.17	1.43	± 0.29	0.85	0.82	0.78
	VAEFit++	0.96	± 0.19	0.96	± 0.20	0.99	± 0.19	0.91	0.89	0.85
Others	Tran <i>et al.</i> [54]	1.93	± 0.27	2.02	± 0.25	1.86	± 0.23	N/A	N/A	N/A
	Booth <i>et al.</i> [6]	1.82	± 0.29	1.85	± 0.22	1.63	± 0.16	N/A	N/A	N/A
	Genova <i>et al.</i> [20]	1.50	± 0.13	1.50	± 0.11	1.48	± 0.11	N/A	N/A	N/A
Ours	<i>GANFit</i> (seed 1)	0.95	± 0.22	0.91	± 0.16	0.95	± 0.18	0.90	0.89	0.87
	<i>GANFit</i> (seed 2)	0.95	± 0.16	0.94	± 0.16	0.97	± 0.18	0.94	0.89	0.87
	<i>GANFit</i> (seed 3)	0.96	± 0.20	0.93	± 0.17	0.94	± 0.18	0.89	0.88	0.87
	<i>Fast-GANFit</i>	1.11	± 0.25	0.98	± 0.15	1.16	± 0.18	0.91	0.89	0.85
	<i>GANFit++</i>	0.94	± 0.17	0.92	± 0.14	0.94	± 0.19	0.94	0.93	0.87
Ablation	$\backslash \mathcal{L}_{id}$	0.96	± 0.18	0.92	± 0.15	0.98	± 0.21	0.93	0.91	0.85
	$\backslash \hat{\mathcal{L}}_{id}$	1.07	± 0.21	1.01	± 0.15	1.05	± 0.23	0.94	0.93	0.87
	$\backslash \mathcal{L}_{con}$	0.94	± 0.17	0.93	± 0.15	0.93	± 0.17	0.93	0.92	0.87
	$\backslash \{\mathcal{L}_{id}, \hat{\mathcal{L}}_{id}, \mathcal{L}_{con}\}$	1.20	± 0.25	1.04	± 0.19	1.18	± 0.25	0.86	0.83	0.78
	$\backslash \mathcal{L}_{lan}$	0.91	± 0.16	0.95	± 0.18	0.93	± 0.17	0.93	0.94	0.91
	$\backslash \mathcal{L}_{pix}$	0.94	± 0.17	0.94	± 0.15	0.93	± 0.19	0.93	0.93	0.87
	$\backslash \text{Reg}\{\mathbf{p}_s\}$	1.03	± 0.18	1.03	± 0.15	1.07	± 0.22	0.94	0.93	0.87
	$\backslash \text{Reg}\{\mathbf{p}_e\}$	0.95	± 0.16	0.93	± 0.14	0.96	± 0.20	0.94	0.93	0.87
	$\backslash \text{Reg}\{\mathbf{p}_l\}$	0.96	± 0.16	0.93	± 0.15	0.94	± 0.20	0.94	0.92	0.87

TABLE 1: Benchmark results on the MICC Florence 3D Faces dataset (MICC) for shape estimation using point-to-plane distance and identity (cosine) similarity between the original frames and the rendered reconstruction. The table reports performance of other methods, the proposed approach including *GANFit* with three different random seeds, the proposed approach with Variational Auto-Encoder (VAE) replacing GAN (names are adjusted accordingly), and leave-one-out ablation study.

combined loss function can effectively optimize the position of the point light source and its color intensities.

Fig. 11 shows 3D reconstruction results given paintings from BAM dataset [59].

5.2.4 *GANFit* vs. *FastGANFit* vs. *GANFit++*

Fig. 7 and 4 demonstrates the estimation by the regression network, namely *FastGANFit*, and the stability improvements by *FastGANFit* initialization, namely *GANFit++*. Please note, although *GANFit* shows an outstanding reconstruction performance, it sometimes fail to converge to a good local minima (as can be seen in *Convergence Plots* in Fig. 7). *FastGANFit* initialization seems to help with that by starting from a easy-to-converge point with more accurate texture, *e.g.* a good judgment against the illumination-skin color ambiguity. Furthermore, *FastGANFit* provides a decent 3D reconstruction estimation under a second, basically faster alternative of *GANFit*.

5.3 Quantitative Experiments

5.3.1 3D shape recovery on MICC dataset

We evaluate the shape reconstruction performance of our method on MICC Florence 3D Faces dataset (MICC) [1] in Table 1. The dataset provides 3D scans of 53 subjects as well as their short video footages under three difficulty settings: ‘cooperative’, ‘indoor’ and ‘outdoor’. Unlike [20], [54] which processes all the frames in a video, we sample only 5 frames from each video. And, we run our method with multi-image support for these 5 frames for each video separately as shown in Eq. 14. Each test mesh is cropped at a radius of 95mm around the tip of the nose according to [54] in order to evaluate the shape recovery of the inner facial mesh. We perform dense alignment between each predicted mesh and its corresponding ground truth mesh, by implementing an iterative closest point (ICP) method [3]. As evaluation metric, we

follow [20] to measure the error by average symetric point-to-plane distance. Additionally, right-most three columns of Table 1 show the cosine similarity between the sampled images and the rendering of their reconstructions.

Table 1 reports the normalized point-to-plain errors in millimeters. It is evident that we have improved the absolute error compared to the other two state-of-the-art methods by 36%. Our results are shown to be consistent across all different settings with minimal standard deviation from the mean error. We also achieve slightly improved and more stable performance by *GANFit++* and still a better reconstruction error by *FastGANFit* compared to other state-of-the-arts.

5.3.2 Experiments on LFW

In order to evaluate identity preservation capacity of the proposed method, we run two face recognition experiments on Labelled Faces in the Wild (LFW) dataset [25]. Following [20], we feed real LFW images and rendered images of their 3D reconstruction by our method to a pretrained face recognition network, namely VGG-Face [34]. We then compute the activations at the embedding layer and measure cosine similarity between 1) real and rendered images and 2) renderings of same/different pairs.

In Fig. 9 and 10, we have quantitatively showed that our method is better at identity preservation and photorealism (*i.e.*, as the pretrained network is trained by real images) than other state-of-the-art deep 3D face reconstruction approaches [20], [54].

5.4 Ablation Study

5.4.1 Analysis on Energy Terms

Fig. 13 shows an ablation study on our method where the full model reconstructs the input face better than its variants, something that suggests that each of our components significantly contributes towards a good reconstruction. Fig. 13(c) indicates albedo is well disentangled from illumination and our model capture the light direction accurately.

While Fig. 13(d-f) shows each of the identity terms contributes to preserve identity, Fig. 13(h) demonstrates the significance identity features altogether. Still, overall reconstruction utilizes pixel intensities to capture better albedo and illumination as shown in Fig. 13(g). Finally, Fig. 13(i) shows the superiority of our textures over PCA-based ones.

From Mean Absolute Errors in Fig. 13, we see that lower pixel loss, as in Fig. 13(h) (0.032), does not bring a good reconstruction. Although Fig. 13(b) has larger pixel intensity difference (0.051), it actually looks drastically more similar to the target identity. We believe that this finding should inspire to design better energy function in the future studies.

In Table 1, we extend this ablation study to MICC dataset to verify the findings quantitatively as well. Most of the results from this experiment are aligned with Fig. 13: 1) identity related loss terms ($\mathcal{L}_{id}, \hat{\mathcal{L}}_{id}, \mathcal{L}_{con}$) recover the absence of one another, however when we exclude all of them, performance drops significantly, 2) Pixel loss (\mathcal{L}_{pix}) only seems to effect illumination/skin color, thus does not change shape reconstruction, 3) On ‘Outdoor’ and ‘Cooperative’ scenarios, however, our method seems to perform better without landmark loss \mathcal{L}_{lan} (given that rough alignment step still includes landmark loss). We believe that this is due to the landmark detector’s failure on low resolution in ‘Outdoor’ setting and extreme poses in ‘Cooperative’ setting. This showcases one of the limitations in our method which is the strong reliance on landmark detector.

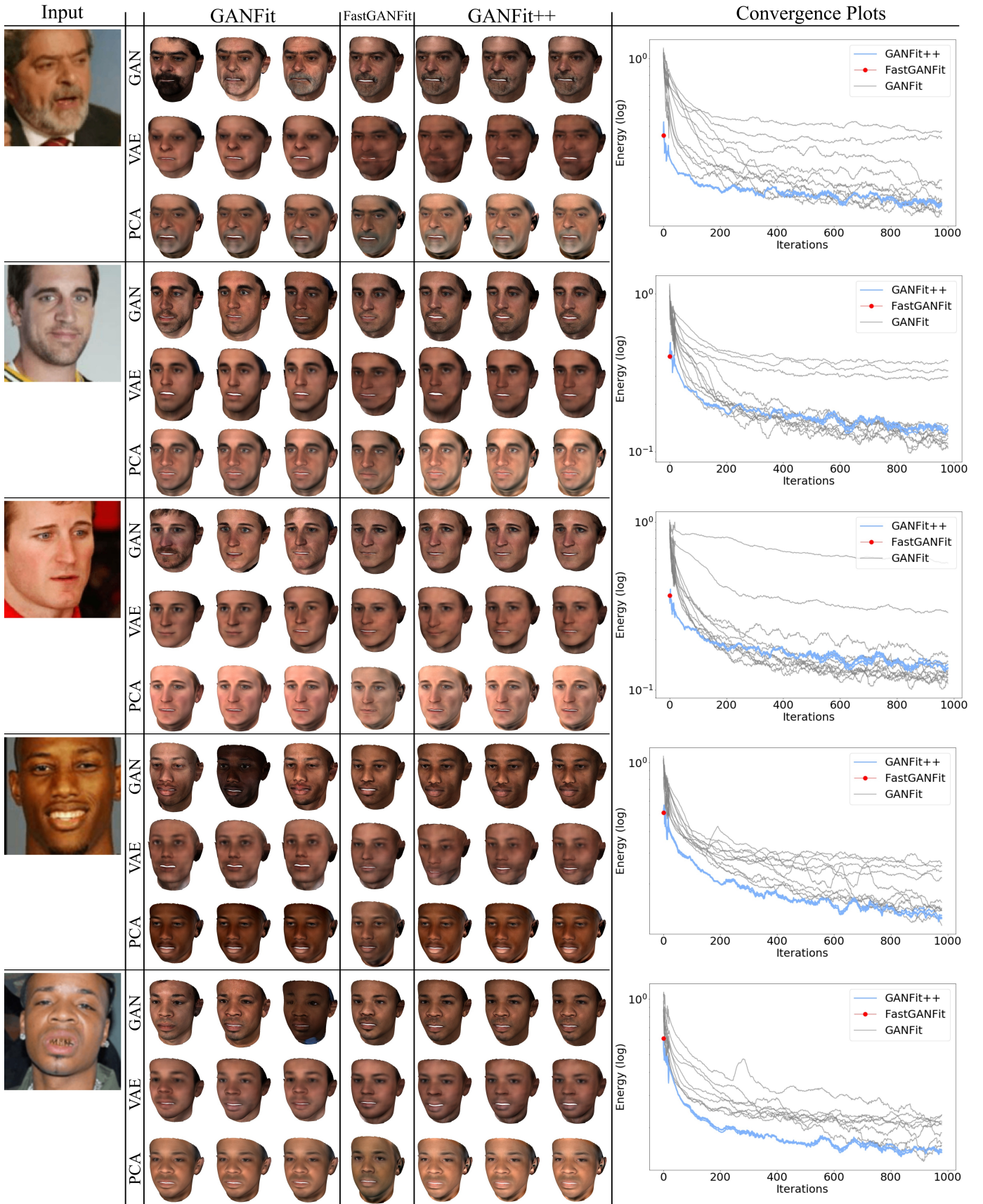


Fig. 7: Qualitative comparison between *GANFit*, *FastGANFit*, *GANFit++* (as mentioned in Sec. 5.2.4) and their variants with Variational Auto-Encoder (VAE) and Principal Component Analysis (PCA) (as mentioned in Sec. 5.4.2) for texture model. *Convergence plots* show the cost function over the iterations of *GANFit* (gray, 10 random initialization), *GANFit++* (blue, 3 random initialization), and initialization by *FastGANFit* (red)

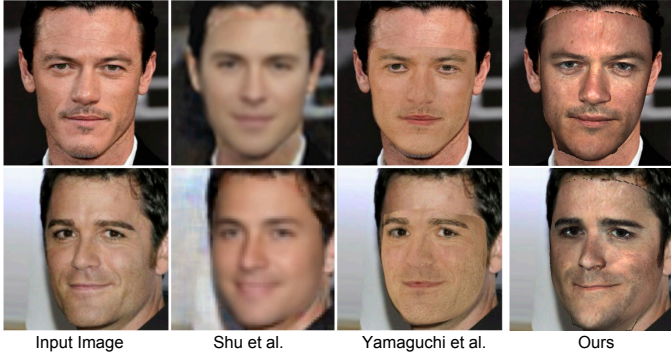


Fig. 8: Qualitative comparison with [46], [61] by overlaying the reconstructions on the input images. Our method can generate high fidelity texture with accurate shape, camera and illumination fitting.

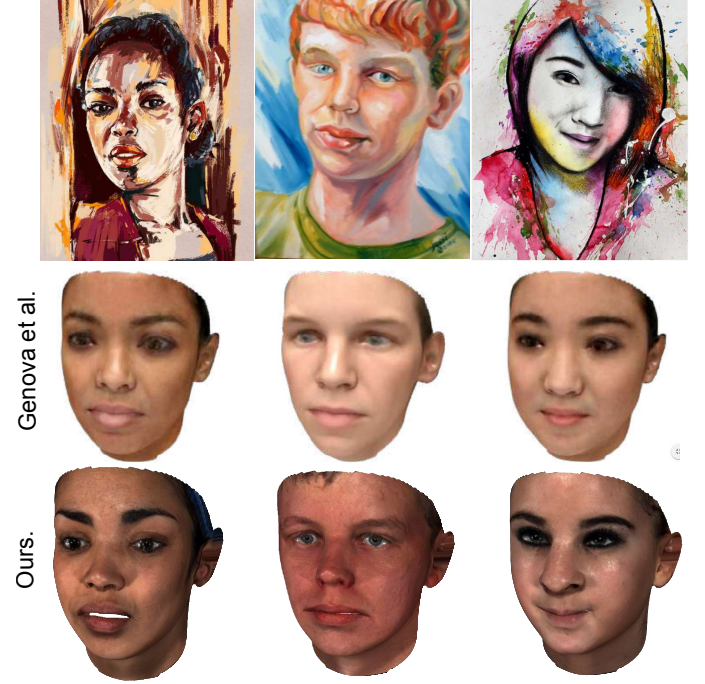


Fig. 11: Our results on BAM dataset [59] compared to [20]. Our method is robust to many image deformations and even capable of recovering identities from paintings thanks to strong identity features.

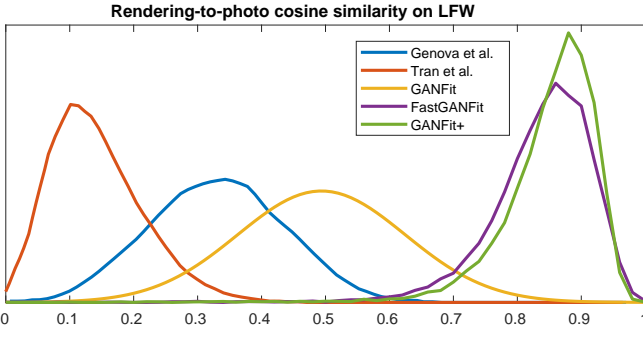


Fig. 9: Cosine similarity distributions of rendered and real images LFW based on activations at the embedding layer of VGG-Face network [34]. Our method achieves more than 0.5 similarity on average which [20] has 0.35 average similarity and [54] 0.16 average similarity.

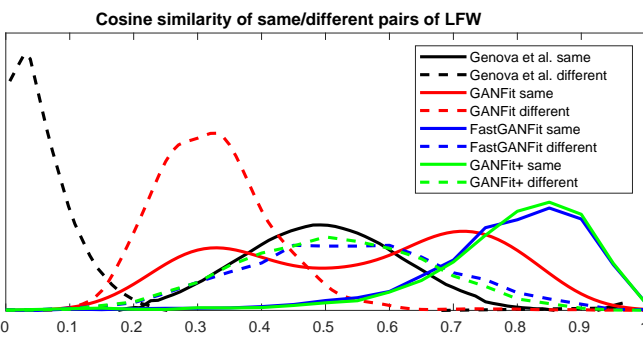


Fig. 10: Our method successfully preserve identity so that distribution of cosine similarity of same/different pairs is separable by thresholding.

Method	Dataset (n. Images)	FID score ↓
GAN [29]	CelebA-HQ (50K)	7.30
NVAE [58]	CelebA-HQ (50K)	40.26
PCA [60]	Ours (9358)	65.80
VAE [31]	Ours (9358)	120.44
NVAE [58]	Ours (9358)	62.98
GAN (Ours) [29]	Ours (9358)	2.95

TABLE 2: Evaluation of various texture models in the UV space by Fréchet Inception Distance (FID) scores. Lower is better.

5.4.2 Analysis on Texture Models

Additionally, we evaluate different texture models in terms of photorealism and diversity of the generations. For this purpose, we implement a commonly used generation quality metric ‘Fréchet Inception Distance’ (FID) and test the performance of Generative Adversarial Networks by [29] as presented in this paper, two variants of Variational Auto-Encoders (VAE) [31], [58] and Principal Component Analysis (PCA) [60], in comparison to the same 10,000 UV texture training set. As shown in Table 2 GAN seems to be performing best among all options for both 2D image generation and 3D UV texture generation, and this justifies the selection of GAN as non-linear texture model compared to all other options. Please also note that moving from 2D dataset to 3D UV textures for GAN also improves the FID score significantly thanks to per-pixel alignment, supporting our argument in Section 3.1

We can confirm these results visually as well in Fig. 7 where texture from GAN is significantly more plausible and high fidelity than the ones from VAE and PCA. Please note that VAE texture model is trained by a vanilla VAE [31] as we couldn’t find a straightforward method to fit with NVAE [58] due to its stochasticity introduced at every resolution level. For both VAE

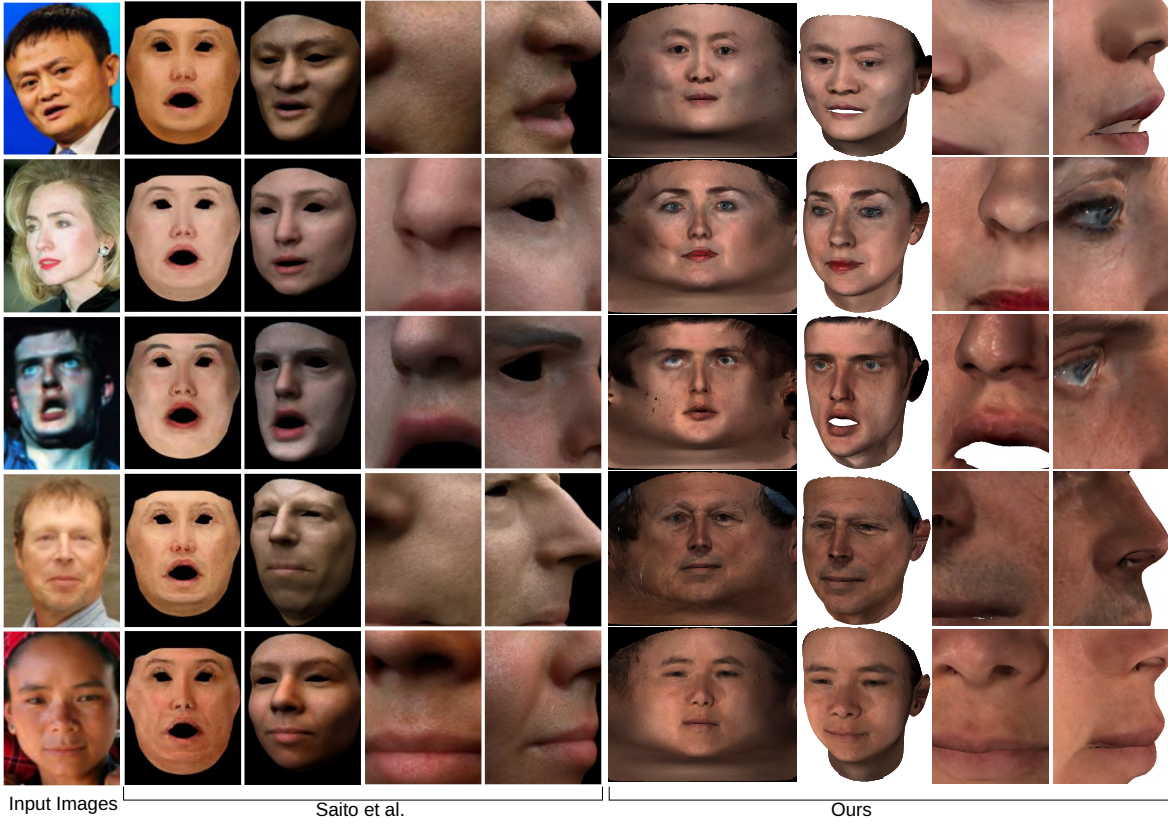


Fig. 12: Qualitative comparison with [42] by means of texture maps, whole and partial face renderings. Please note that while our method does not require any particular renderer for special effects, *e.g.*, lighting, it can produce comparable results to [42] which renders its results by a commercial renderer called Arnold.

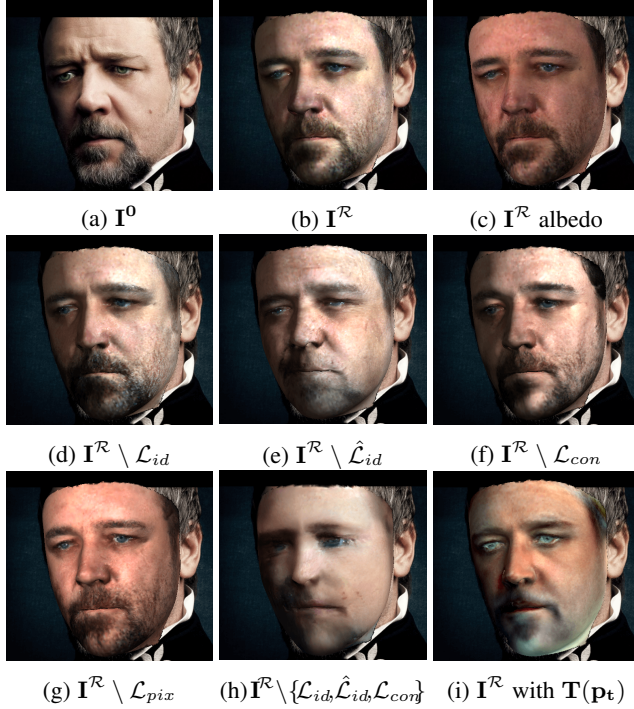


Fig. 13: Contributions of the components or loss terms of the proposed approach with an leave-one-out ablation study. Mean Absolute Errors of (b-i) w.r.t. (a) are as follows respectively: 0.051, 0.114, 0.053, 0.054, 0.063, 0.099, 0.032, 0.064.

and PCA results, the rest of the implementation is kept the same as the original proposed approach, *i.e.*, similar regression network trained for VAE and PCA models.

6 CONCLUSION

In this paper, we revisit optimization-based 3D face reconstruction under a new perspective, that is, we utilize the power of recent machine learning techniques such as GANs and face recognition network as statistical texture model and as energy function respectively. Later, we stabilize and expedite this approach by training a regression network for 3D face reconstruction by the same pipeline in a self-supervised fashion.

To the best of our knowledge, this is the first time that GANs are used for model fitting and they have shown excellent results for high quality texture reconstruction. The proposed approach shows identity preserving high fidelity 3D reconstructions in qualitative and quantitative experiments.

ACKNOWLEDGMENTS

Stefanos Zafeiriou acknowledges support by EPSRC Fellowship DEFORM (EP/S010203/1) and a Google Faculty Award.

REFERENCES

- [1] Andrew D Bagdanov, Alberto Del Bimbo, and Iacopo Masi. The florence 2d/3d hybrid face dataset. In *Proceedings of the 2011 joint ACM workshop on Human gesture and behavior understanding*, pages 79–80. ACM, 2011. 9

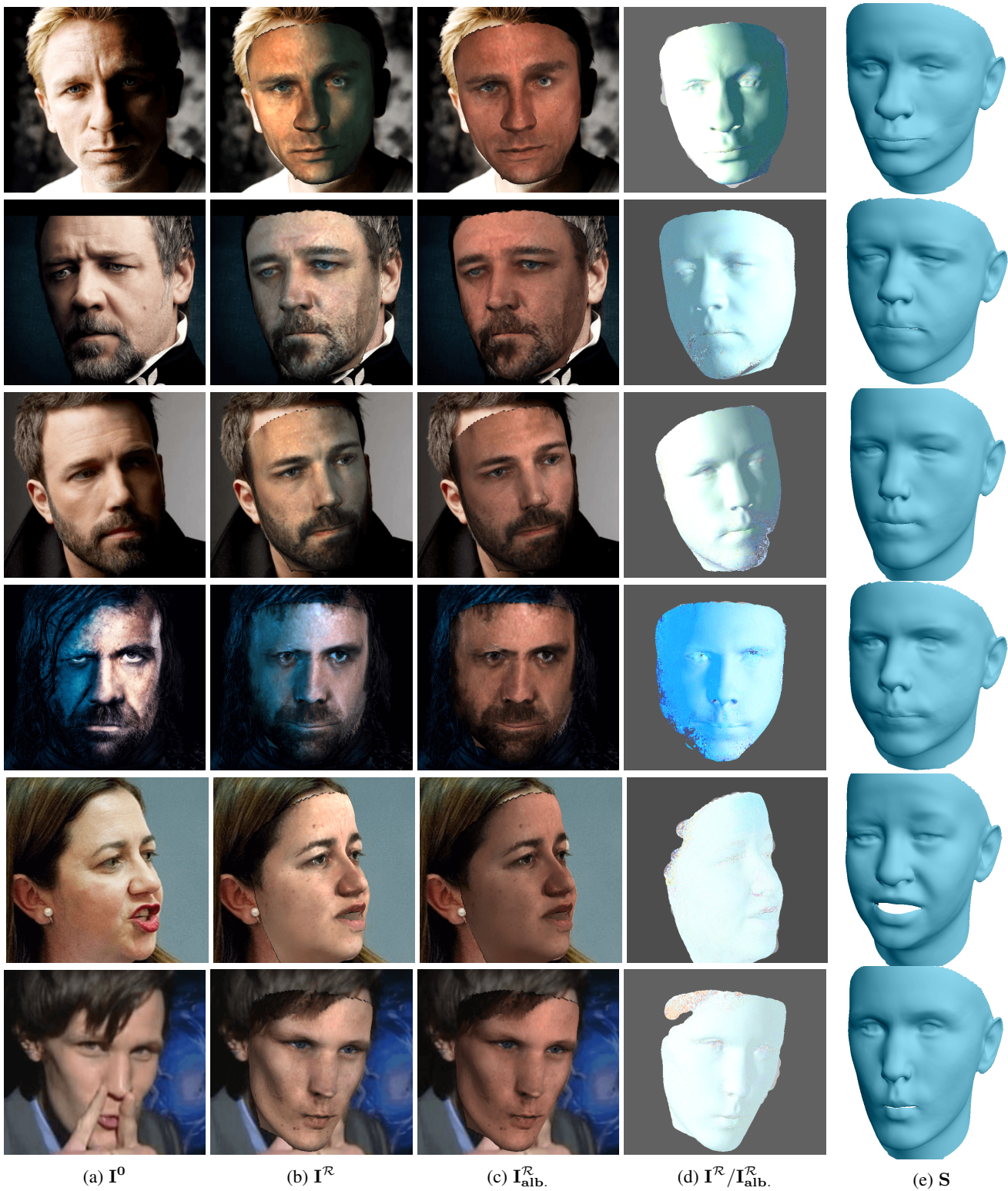


Fig. 14: Results under more challenging conditions, *i.e.* strong illuminations, self-occlusions and facial hair. (a) Input image. (b) Estimated fitting overlayed including illumination estimation. (c) Overlayed fitting without illumination. (d) Normalized pixel-wise intensity ratio of (b) to (c). (e) Estimated shape mesh

[2] Anil Bas, William AP Smith, Timo Bolkart, and Stefanie Wuhrer. Fitting a 3d morphable model to edges: A comparison between hard and soft correspondences. In *ACCV*, 2016. 3

[3] Paul J Besl and Neil D McKay. Method for registration of 3-d shapes. In *Sensor Fusion IV: Control Paradigms and Data Structures*, volume 1611, pages 586–607, 1992. 9

[4] Volker Blanz and Thomas Vetter. A morphable model for the synthesis of 3d faces. In *Proceedings of the 26th annual conference on Computer graphics and interactive techniques*, pages 187–194. ACM Press/Addison-Wesley Publishing Co., 1999. 1

[5] Volker Blanz and Thomas Vetter. Face recognition based on fitting a 3d morphable model. *TPAMI*, 25(9):1063–1074, 2003. 3

[6] James Booth, Epameinondas Antonakos, Stylianos Ploumpis, George Trigeorgis, Yannis Panagakis, Stefanos Zafeiriou, et al. 3d face morphable models “in-the-wild”. In *CVPR*, 2017. 1, 3, 9

[7] James Booth, Anastasios Roussos, Stefanos Zafeiriou, Allan Ponniah, and David Dunaway. A 3d morphable model learnt from 10,000 faces. In *CVPR*, 2016. 1, 6

[8] Shiyang Cheng, Irene Kotsia, Maja Pantic, and Stefanos Zafeiriou. 4dfab: a large scale 4d facial expression database for biometric applications. *arXiv preprint arXiv:1712.01443*, 2017. 6

[9] Forrester Cole, David Belanger, Dilip Krishnan, Aaron Sarna, Inbar Mosseri, and William T Freeman. Synthesizing normalized faces from facial identity features. In *CVPR*, 2017. 1, 5

[10] Hang Dai, Nick Pears, William Smith, and Christian Duncan. A 3d morphable model of craniofacial shape and texture variation. In *2017 IEEE International Conference on Computer Vision (ICCV)*, 2017. 1

[11] Jiankang Deng, Shiyang Cheng, Niannan Xue, Yuxiang Zhou, and Stefanos Zafeiriou. Uv-gan: Adversarial facial uv map completion for pose-invariant face recognition. *CVPR*, 2018. 2

[12] Jiankang Deng, Jia Guo, and Stefanos Zafeiriou. Arcface: Additive angular margin loss for deep face recognition. *arXiv preprint arXiv:1801.07698*, 2018. 2, 3, 5, 6

[13] Jiankang Deng, Yuxiang Zhou, Shiyang Cheng, and Stefanos Zafeiriou. Cascade multi-view hourglass model for robust 3d face alignment. In *Automatic Face & Gesture Recognition (FG)*, pages 399–403. IEEE, 2018. 3, 5, 6

[14] Bernhard Egger, William AP Smith, Ayush Tewari, Stefanie Wuhrer, Michael Zollhoefer, Thabo Beeler, Florian Bernard, Timo Bolkart, Adam Kortylewski, Sami Romdhani, et al. 3d morphable face models—past, present, and future. *ACM Transactions on Graphics (TOG)*, 39(5):1–38, 2020. 1

[15] Pablo Garrido, Michael Zollhöfer, Dan Casas, Levi Valgaerts, Kiran Varanasi, Patrick Pérez, and Christian Theobalt. Reconstruction of personalized 3d face rigs from monocular video. *ACM Transactions on Graphics (TOG)*, 35(3):28, 2016. 1, 3

[16] Baris Gecer, Binod Bhattacharai, Josef Kittler, and Tae-Kyun Kim. Semi-supervised adversarial learning to generate photorealistic face images of new identities from 3d morphable model. *ECCV*, 2018. 5

[17] Baris Gecer, Jiankang Deng, and Stefanos Zafeiriou. Ostec: One-shot texture completion. In *Proceedings of the IEEE/CVF Conference on Computer Vision and Pattern Recognition*, 2021. 2

[18] Baris Gecer, Alexandros Lattas, Stylianos Ploumpis, Jiankang Deng, Athanasios Papaioannou, Stylianos Moschoglou, and Stefanos Zafeiriou. Synthesizing coupled 3d face modalities by trunk-branch generative adversarial networks. In *European Conference on Computer Vision*, pages 415–433. Springer, 2020. 1

[19] Baris Gecer, Stylianos Ploumpis, Irene Kotsia, and Stefanos Zafeiriou. Ganfit: Generative adversarial network fitting for high fidelity 3d face reconstruction. In *Proceedings of the IEEE Conference on Computer Vision and Pattern Recognition*, pages 1155–1164, 2019. 2

[20] Kyle Genova, Forrester Cole, Aaron Maschinot, Aaron Sarna, Daniel Vlasic, and William T Freeman. Unsupervised training for 3d morphable model regression. In *CVPR*, 2018. 1, 4, 5, 6, 7, 8, 9, 11

[21] Ian Goodfellow. Nips 2016 tutorial: Generative adversarial networks. *arXiv preprint arXiv:1701.00160*, 2016. 3

[22] Yudong Guo, Juyong Zhang, Jianfei Cai, Boyi Jiang, and Jianmin Zheng. Cnn-based real-time dense face reconstruction with inverse-rendered photo-realistic face images. *IEEE transactions on pattern analysis and machine intelligence*, 2018. 1

[23] Kaiming He, Xiangyu Zhang, Shaoqiang Ren, and Jian Sun. Deep residual learning for image recognition. In *CVPR*, 2016. 6

[24] Guosheng Hu, Fei Yan, Josef Kittler, William Christmas, Chi Ho Chan, Zhenhua Feng, and Patrik Huber. Efficient 3d morphable face model fitting. *Pattern Recognition*, 67:366–379, 2017. 3

[25] Gary B. Huang, Marwan Mattar, Honglak Lee, and Erik Learned-Miller. Learning to align from scratch. In *NIPS*, 2012. 9

[26] IEEE. *A 3D Face Model for Pose and Illumination Invariant Face Recognition*, 2009. 1

[27] Luo Jiang, Juyong Zhang, Bailin Deng, Hao Li, and Ligang Liu. 3d face reconstruction with geometry details from a single image. *IEEE Transactions on Image Processing*, 27(10):4756–4770, 2018. 1

[28] Ian Jolliffe. Principal component analysis. In *International encyclopedia of statistical science*, pages 1094–1096. Springer, 2011. 3

[29] Tero Karras, Timo Aila, Samuli Laine, and Jaakko Lehtinen. Progressive growing of GANs for improved quality, stability, and variation. In *ICLR*, 2018. 4, 6, 11

[30] Diederik P Kingma and Jimmy Ba. Adam: A method for stochastic optimization. *arXiv preprint arXiv:1412.6980*, 2014. 6

[31] Diederik P. Kingma and Max Welling. Auto-encoding variational bayes. *2nd International Conference on Learning Representations, ICLR 2014 - Conference Track Proceedings*, 2014. 11

[32] Alexandros Lattas, Stylianos Moschoglou, Baris Gecer, Stylianos Ploumpis, Vasileios Triantafyllou, Abhijeet Ghosh, and Stefanos Zafeiriou. Avatarme: Realistically renderable 3d facial reconstruction “in-the-wild”. In *Proceedings of the IEEE/CVF Conference on Computer Vision and Pattern Recognition*, pages 760–769, 2020. 1

[33] Stephen Lombardi, Jason Saragih, Tomas Simon, and Yaser Sheikh. Deep appearance models for face rendering. *ACM Transactions on Graphics (TOG)*, 37(4):68, 2018. 1

[34] O. M. Parkhi, A. Vedaldi, and A. Zisserman. Deep face recognition. In *British Machine Vision Conference*, 2015. 9, 11

[35] Omkar M Parkhi, Andrea Vedaldi, Andrew Zisserman, et al. Deep face recognition. In *BMVC*, 2015. 3

[36] Marcel Piotraschke and Volker Blanz. Automated 3d face reconstruction from multiple images using quality measures. In *CVPR*, 2016. 3

[37] Stylianos Ploumpis, Evangelos Ververas, Eimear O’Sullivan, Stylianos Moschoglou, Haoyang Wang, Nick Pears, William Smith, Baris Gecer, and Stefanos P Zafeiriou. Towards a complete 3d morphable model of the human head. *IEEE transactions on pattern analysis and machine intelligence*, 2020. 1

[38] Elad Richardson, Matan Sela, and Ron Kimmel. 3d face reconstruction by learning from synthetic data. In *2016 Fourth International Conference on 3D Vision (3DV)*, pages 460–469. IEEE, 2016. 1

[39] Elad Richardson, Matan Sela, Roy Or-El, and Ron Kimmel. Learning detailed face reconstruction from a single image. In *CVPR*, 2017. 1

[40] Sami Romdhani, Volker Blanz, and Thomas Vetter. Face identification by fitting a 3d morphable model using linear shape and texture error functions. In *ECCV*, 2002. 3

[41] Sami Romdhani and Thomas Vetter. Estimating 3d shape and texture using pixel intensity, edges, specular highlights, texture constraints and a prior. In *CVPR*, 2005. 1, 3

[42] Shunsuke Saito, Lingyu Wei, Liwen Hu, Koki Nagano, and Hao Li. Photorealistic facial texture inference using deep neural networks. In *CVPR*, 2017. 1, 7, 12

[43] Soubhik Sanyal, Timo Bolkart, Haiwen Feng, and Michael J Black. Learning to regress 3d face shape and expression from an image without 3d supervision. In *Proceedings of the IEEE/CVF Conference on Computer Vision and Pattern Recognition*, pages 7763–7772, 2019. 1

[44] Florian Schroff, Dmitry Kalenichenko, and James Philbin. Facenet: A unified embedding for face recognition and clustering. In *CVPR*, 2015. 3

[45] Matan Sela, Elad Richardson, and Ron Kimmel. Unrestricted facial geometry reconstruction using image-to-image translation. In *ICCV*, 2017. 1

[46] Zhixin Shu, Ersin Yumer, Sunil Hadap, Kalyan Sunkavalli, Eli Shechtman, and Dimitris Samaras. Neural face editing with intrinsic image disentangling. In *Computer Vision and Pattern Recognition (CVPR), 2017 IEEE Conference on*, pages 5444–5453. IEEE, 2017. 11

[47] Ron Slossberg, Gil Shamai, and Ron Kimmel. High quality facial surface and texture synthesis via generative adversarial networks. *ECCVW*, 2018. 2

[48] William AP Smith, Alassane Seck, Hannah Dee, Bernard Tiddeman, Joshua B Tenenbaum, and Bernhard Egger. A morphable face albedo model. In *Proceedings of the IEEE/CVF Conference on Computer Vision and Pattern Recognition*, pages 5011–5020, 2020. 1

[49] Ayush Tewari, Florian Bernard, Pablo Garrido, Gaurav Bharaj, Mohamed Elgarhib, Hans-Peter Seidel, Patrick Pérez, Michael Zollhoefer, and Christian Theobalt. Fml: Face model learning from videos. In *Proceedings of the IEEE/CVF Conference on Computer Vision and Pattern Recognition*, pages 10812–10822, 2019. 1

[50] Ayush Tewari, Michael Zollhoefer, Florian Bernard, Pablo Garrido, Hyeongwoo Kim, Patrick Perez, and Christian Theobalt. High-fidelity monocular face reconstruction based on an unsupervised model-based face autoencoder. *IEEE transactions on pattern analysis and machine intelligence*, 42(2):357–370, 2018. 1

[51] Ayush Tewari, Michael Zollhöfer, Pablo Garrido, Florian Bernard, Hyeongwoo Kim, Patrick Pérez, and Christian Theobalt. Self-supervised multi-level face model learning for monocular reconstruction at over 250 hz. 2018. 1, 3, 7, 8

- [52] Ayush Tewari, Michael Zollhöfer, Hyeongwoo Kim, Pablo Garrido, Florian Bernard, Patrick Pérez, and Christian Theobalt. Mofa: Model-based deep convolutional face autoencoder for unsupervised monocular reconstruction. In *ICCV*, 2017. [1](#), [7](#), [8](#)
- [53] Justus Thies, Michael Zollhofer, Marc Stamminger, Christian Theobalt, and Matthias Nießner. Face2face: Real-time face capture and reenactment of rgb videos. In *CVPR*, pages 2387–2395, 2016. [1](#)
- [54] Anh Tuan Tran, Tal Hassner, Iacopo Masi, and Gérard Medioni. Regressing robust and discriminative 3d morphable models with a very deep neural network. In *CVPR*, 2017. [1](#), [6](#), [7](#), [8](#), [9](#), [11](#)
- [55] Luan Tran, Feng Liu, and Xiaoming Liu. Towards high-fidelity nonlinear 3d face morphable model. In *Proceedings of the IEEE/CVF Conference on Computer Vision and Pattern Recognition*, pages 1126–1135, 2019. [1](#)
- [56] Luan Tran and Xiaoming Liu. Nonlinear 3d face morphable model. In *CVPR*, 2018. [1](#), [3](#), [7](#), [8](#)
- [57] Luan Tran and Xiaoming Liu. On learning 3d face morphable model from in-the-wild images. *IEEE transactions on pattern analysis and machine intelligence*, 43(1):157–171, 2019. [1](#)
- [58] Arash Vahdat and Jan Kautz. Nvae: A deep hierarchical variational autoencoder. *arXiv preprint arXiv:2007.03898*, 2020. [11](#)
- [59] Michael J Wilber, Chen Fang, Hailin Jin, Aaron Hertzmann, John Collomosse, and Serge J Belongie. Bam! the behance artistic media dataset for recognition beyond photography. In *ICCV*, pages 1211–1220, 2017. [9](#), [11](#)
- [60] Svante Wold, Kim Esbensen, and Paul Geladi. Principal component analysis. *Chemometrics and Intelligent Laboratory Systems*, 2(1):37–52, 1987. [11](#)
- [61] Shuho Yamaguchi, Shunsuke Saito, Koki Nagano, Yajie Zhao, Weikai Chen, Kyle Olszewski, Shigeo Morishima, and Hao Li. High-fidelity facial reflectance and geometry inference from an unconstrained image. *ACM Transactions on Graphics (TOG)*, 37(4):162, 2018. [1](#), [11](#)
- [62] Xiangyu Zhu, Zhen Lei, Xiaoming Liu, Hailin Shi, and Stan Z Li. Face alignment across large poses: A 3d solution. In *CVPR*, 2016. [1](#)



Baris Gecer is currently working as a Senior Research Scientist in the industry. He has received his PhD. degree from the Department of Computing, Imperial College London in 2020, under the supervision of Prof. Stefanos Zafeiriou. Previously, he was a Research Intern at Facebook Reality Labs, supervised by Dr. Fernando De La Torre. He obtained his M.Sc. degree from Bilkent University Computer Engineering department under the supervision of Dr. Selim Aksoy in 2016 and obtained his undergraduate degree in Computer Engineering from Hacettepe University in 2014. His main research interests are photorealistic 3D Face reconstruction, modeling, and synthesis by Generative Adversarial Nets and Deep Learning.



Stylianos Ploumpis received the Diploma and Master of Engineering in Production Engineering & Management from Democritus University of Thrace, Greece (D.U.T.H.), in 2013. He joined the department of computing at Imperial College London, in October 2015, where he pursued an MSc in Computing specialising in Machine Learning. Currently, he is a PhD candidate/Researcher at the Department of Computing at Imperial College, under the supervision of Dr. Stefanos Zafeiriou. His research interests lie in the field of 3D Computer Vision, Pattern Recognition and Machine Learning.



Irene Kotsia received the Ph.D. degree from the Department of Informatics, Aristotle University of Thessaloniki, Thessaloniki, Greece, in 2008. From 2008 to 2009 she was a Research Associate and teaching assistant in the department of Informatics at Aristotle University of Thessaloniki. From 2009 to 2011 she was a Research Associate in the department of Electronic Engineering and Computer Science of Queen Mary University of London, while from 2012 to 2014 she was a Senior Research Associate in the department of computing in Imperial College London. She was the recipient of the Action Supporting Postdoctoral Researchers of the Operational Program Education and Lifelong Learning (Actions Beneficiary: General Secretariat for Research and Technology) fellowship from 2012 to 2015. From 2013 to 2015 she was a Lecturer in Creative Technology and Digital Creativity in the department of Computing Science of Middlesex University of London, where she is now a Senior Lecturer. She has been a Guest Editor of two journal special issues dealing with face analysis topics (in Computer Vision and Image Understanding and IEEE Transactions on Cybernetics journals). She has co-authored more than 40 journal and conference publications in the most prestigious journals and conferences of her field (e.g., IEEE T-IP, IEEE T-NNLS, CVPR, ICCV).



Stefanos Zafeiriou is currently a Reader in Machine Learning and Computer Vision with the Department of Computing, Imperial College London, London, U.K, and a Distinguishing Research Fellow with University of Oulu under Finish Distinguishing Professor Programme. He also holds an EPSRC Fellowship. He was a recipient of the Prestigious Junior Research Fellowships from Imperial College London in 2011 to start his own independent research group. He was the recipient of the President's Medal for Excellence in Research Supervision for 2016. He has received various awards during his doctoral and post-doctoral studies. He currently serves as an Associate Editor of the IEEE Transactions on Affective Computing and Computer Vision and Image Understanding journal. In the past he held editorship positions in IEEE Transactions on Cybernetics, the Image and Vision Computing Journal. He has been a Guest Editor of over six journal special issues and co-organised over 13 workshops/special sessions on specialised computer vision topics in top venues, such as CVPR/FG/ICCV/ECCV (including three very successfully challenges run in ICCV'13, ICCV'15 and CVPR'17 on facial landmark localisation/tracking). He has co-authored over 55 journal papers mainly on novel statistical machine learning methodologies applied to computer vision problems, such as 2-D/3-D face analysis, deformable object fitting and tracking, shape from shading, and human behaviour analysis, published in the most prestigious journals in his field of research, such as the IEEE T-PAMI, the International Journal of Computer Vision, the IEEE T-IP, the IEEE T-NNLS, the IEEE T-VCG, and the IEEE T-IFS, and many papers in top conferences, such as CVPR, ICCV, ECCV, ICML. His students are frequent recipients of very prestigious and highly competitive fellowships, such as the Google Fellowship x2, the Intel Fellowship, and the Qualcomm Fellowship x3. He has more than 10K citations to his work, h-index 50. He is the General Chair of BMVC 2017.